

# Impact of Flow Conditions and Geometrical Parameters on the Separation of Two Immiscible Liquids in Helical Pipes

Michael Mansour<sup>1,2\*</sup>, Conrad Müller<sup>2</sup>, Dominique Thévenin<sup>2</sup>, and Katharina Zähringer<sup>2</sup>

<sup>1</sup> Mechanical Power Engineering Department, Faculty of Engineering - Mataria, Helwan University, 11718 Cairo, Egypt.

<sup>2</sup> Lab. of Fluid Dynamics & Technical Flows, University of Magdeburg “Otto von Guericke”, 39106 Magdeburg, Germany.

**Abstract:** The separation of two immiscible liquids was studied in helical pipes with different flow and geometrical conditions. The main objective is to investigate the impact of the geometrical dimensions on the phase separation in helical pipes. The Volume Of Fluid (VOF) method was used to model the two-phase flow. The separation performance was quantified and compared using the average mixing coefficient of the two liquids. A perfect mixture of two liquids (water and amine) was always assumed at the inlet. Comparing different flow orientations, proper separation could only be obtained when the helical pipe is oriented horizontally. A laminar flow at the optimal range of Reynolds number for separation was considered (approximately  $Re = 225-563$ ), where  $Re = 225$  leads to a slightly better separation. The three key geometrical dimensions of helical pipes; the coil pitch, the pipe diameter, and the coil diameter were studied within the ranges of 16–60 mm, 5–15 mm, and 70–150 mm, respectively. The results show that changing the coil pitch has no significant effect on the separation behavior, while high enough pipe and coil diameters are needed to preserve an efficient separation of immiscible liquids and easier extraction of the lighter phase.

**Keywords:** Liquid-liquid separation, Helical pipes, Immiscible liquids, Impact of geometrical conditions, Computational Fluid Dynamics (CFD), Volume Of Fluid (VOF)

## Nomenclature

### Roman symbols

$A$	cross-sectional area [m <sup>2</sup> ]
$A_f$	grid face area [m <sup>2</sup> ]
$D$	coil diameter [m]
$d$	pipe diameter [m]
$\bar{V}$	Average volume of computational cell [m <sup>3</sup> ]
$f_b$	body force [N]
$g$	gravitational acceleration [m/s <sup>2</sup> ]
$i$	unit vector of Cartesian axes [-]
$k$	number of fluid phases [-]
$L$	length of coil [m]
$M_c$	mixing coefficient [-]
$n$	number of turns [-]
$P$	coil pitch [m]
$p$	pressure [N/m <sup>2</sup> ]
$u$	flow velocity [m/s]
$V$	volume of computational cell [m <sup>3</sup> ]
$v$	average flow velocity [m/s]
$V_m$	volume of phase $m$ [m <sup>3</sup> ]
$X/L$	dimensionless axial length [-]
CFL	Courant–Friedrichs–Lewy number [-]

$De_a$	superficial Dean number of amine ( $Re_a \sqrt{\delta}$ )
$De_w$	superficial Dean number of water ( $Re_w \sqrt{\delta}$ )
$Re_a$	superficial Reynolds number of amine [-]
$Re_w$	superficial Reynolds number of water [-]

### Greek symbols

$\alpha$	volume fraction [-]
$\alpha_m$	local grid volume fraction of phase $m$ [-]
$\gamma$	Dimensionless pitch ( $P/\pi D$ )
$\bar{\alpha}_m$	surface-averaged volume fraction of phase $m$ [-]
$\delta$	curvature ratio ( $d/D$ )
$\mu$	dynamic viscosity [Pa s]
$\mu_a$	dynamic viscosity of amine [Pa s]
$\mu_m$	dynamic viscosity of phase $m$ [Pa s]
$\mu_w$	dynamic viscosity of water [Pa s]
$\rho$	density [kg/m <sup>3</sup> ]
$\rho_a$	density of amine [kg/m <sup>3</sup> ]
$\rho_m$	density of phase $m$ [kg/m <sup>3</sup> ]
$\rho_w$	density of water [kg/m <sup>3</sup> ]
$\theta$	coil angle measured from inlet surface of the coil [°]

## 1 Introduction

Centrifugal forces are created in helical (coiled) pipes thanks to the fluid movement in a curved path, producing a secondary flow of vortices in the radial direction (Dean vortices) (Dean, 1927). The performance of many processes in helical pipes is enhanced accordingly, such as flow mixing, residence time distributions, as well as heat and mass transfers when they are compared to those of straight pipes (Acharya et al., 1992; Gelfgat et al., 2003; Liu et al., 2005; Jokiel et al., 2017; Mansour et al., 2017, 2018; Kováts et al., 2018; Mansour et al., 2020a,b, 2019b). Additionally, multiple advantages are gained by employing helical pipes. For instance, they have a compact design, do not engage any moving components, and require no power source. Therefore, minimal maintenance and energy consumption are needed. Nonetheless, a higher pressure drop usually occurs in the helical pipe compared to a straight pipe with a similar length (Mansour et al., 2020a).

Immiscible (non-miscible) fluid flow is a significant Multiphase flow type for several chemical and physical applications, compromising, for instance, petroleum, food, oil, pharmaceutical, nuclear, and polymer industries (Vashisth et al., 2008). Such flows may include gas-liquid or liquid-liquid flows. Immiscible fluids flow may also be very intricate, depending on the involved phases' characteristics, their volume fractions, and the flow regime type (e.g., disperse, slug, plug, segregated...). Moreover, the existence of both the centrifugal force and Dean vortices in helical pipes increases the complexity when these flows are studied (Mansour et al., 2020b).

In the literature, numerous studies for flows in helical pipes are available regarding miscible fluids (Jiang et al., 2004; Kumar et al., 2006; Vanka et al., 2004; Mansour et al., 2017, 2020a, 2019b; Khot et al., 2019; Mansour et al., 2020g,f) together with immiscible fluids (Mansour et al., 2020b; Brauner and Maron, 1992; Ali and Mandal, 2019; Gelfgat et al., 2003; Zhang et al., 2006, 2014). Mainly, the general flow properties, the formation and the structure of Dean vortices, the flow mixing, residence time distributions, and the improvement of mass and heat transfer are all very common objectives for the investigations concerning miscible fluids flow in helical pipes. Correspondingly, various aims are pursued in the investigations of immiscible fluids flow in helical pipes. For example, the possible improvement of mass transfer between immiscible liquids in a curved pipe was the focus in Gelfgat et al. (2003). It was shown that the strength of the secondary flow does not always improve when increasing the Reynolds number ( $Re$ ). Instead, for considered flow and geometrical dimensions in Gelfgat et al. (2003), a value of  $Re = 50$  was identified as the best value of the Reynolds number for maximizing the mass transfer between the liquids.

The flow patterns and distributions of phases of immiscible liquid-liquid flows in helical and curved pipes were analyzed in detail in several previous studies. In Sharma et al. (2011), an immiscible flow of water and kerosene in curved return bends was considered. The flow patterns were classified into stratified, plug, and dispersed flow. In this study, the pipe orientation (upward, downward, or horizontal) played no significant role concerning the flow patterns. However, this might be only due to the very short pipe length employed in the study (half of a coil turn). In Pietrzak (2014); Ali and Mandal (2019), other flow patterns were identified experimentally, such as dispersed (drops), wavy, plugs, stratified and annular-dispersed flows. These studies confirmed that the flow regimes in helical pipes are distinguishable from those of straight pipes. Additionally, the viscosity was found to be a significant parameter concerning the flow patterns (Ali and Mandal, 2019). Still, abundant flow patterns were additionally observed in some recent studies for immiscible flows in curved pipes according to the considered flow conditions and geometrical parameters (Al-Azzawi et al., 2021).

Several applications and processes necessitate the separation of fluid phases, involving for instance oil and pharmaceutical industries (Weiwei et al., 2020). Separation of phases is mainly required to achieve isolation, extraction, purification, reuse, or recovery of one or more of the phases. However, the task of separating immiscible fluids is not simple as soon as the fluids are allowed to be in contact. Examples of established separation methods are distillation (Hartman et al., 2009), chromatography (Culbertson et al., 2000), filtration (Juang et al., 2019), centrifugation (von Deylen et al., 2022), and gravity settling (Steinhoff et al., 2021). These methods depend on various forces acting on the fluids such as buoyant, centrifugal, surface tension, capillary, viscous, and/or gravitational force. Some methods involve combinations of different forces to achieve separation of fluid phases (da Mota and Pagano, 2014). Accordingly, many separation systems were developed as found in the literature. Nevertheless, most of these systems involve one or more disadvantages. For instance, most separation systems available have an intricate design, can be only used in restricted applications, or are not developed for continuous processes.

Alternatively, the several advantages of helical pipes (e.g., the compact and simple structure) were also utilized for the separation of fluid phases in several investigations. In Zhang et al. (2006); Xu et al. (2020), investigations were done for the separation of oil and water flows in helical pipes. Within the considered flow conditions and geometrical dimensions, the results stated that the separation process can be enhanced by increasing the diameter of the water droplets, increasing the flow rate of the flow, or decreasing the curvature ratio of the coil (Zhang et al., 2006; Xu et al., 2020). Still, this is not valid generally for different flow conditions and geometrical dimensions because of the non-monotonic change of the structure of Dean vortices when increasing the flow rate of the flow (Mansour et al., 2017, 2020a; Kováts et al., 2020a,b). This was approved in separation studies of gas and liquid flows in helical pipes, where the relationship between separation and flow rate changes trend based on the flow rate range (Zhang et al., 2014; da Mota and Pagano, 2014).

In Zhang et al. (2014), three various trends of separation were observed when the fluid velocity is increased. Again, the reason for this variable trend and non-monotonic change in the separation efficiency with the flow rate (the flow velocity) is that the increase of the flow velocity changes not only the structure of the secondary flow but also the magnitude of different forces as well as the residence time available for the process. Accordingly, the flow rate (flow conditions) should be optimized for achieving the best separation efficiency for immiscible fluids in helical pipes. Though important conclusions are delivered, most of the former investigations are limited concerning one or more aspects. For instance, the studies available considered very short pipe lengths (part of a coil turn), a single flow direction (vertical or horizontal), an individual measurement position (mostly the pipe outlet), restricted flow conditions, or simple/unpractical inlet conditions.

In light of the previous discussions, the present work aims to study the separation of immiscible liquids in helical pipes filling several of the mentioned gaps in the literature. Common and practical inlet conditions are assumed at the inlet, i.e., the fluids are totally dispersed in one another (perfectly mixed). In our previous work (Mansour et al., 2021), the separation performance of amine and water (immiscible liquids) in helical and straight pipes was investigated. Only very weak separation occurred in straight pipes also for different orientations. However, reliable separation could be achieved when employing a helical pipe in a horizontal orientation. The best separation occurred within the optimal range of water Reynolds number of approximately  $Re_w=225-563$ . Nevertheless, in this previous study only fixed geometrical parameters for an individual helical pipe were considered, restricting the validity of the results.

Further, the geometrical dimensions may strongly impact the intensity and the structure of the developed secondary flow in the pipes (Dean, 1927; Liou, 1992; Tang et al., 2016, 2017). For instance, the increase of the coil pitch ( $P$ ) was found to change the shape of the developed vortices (Mishra and Gupta, 1979; Hüttel and Friedrich, 2000, 2001; Yamamoto et al., 1994). For very high values of coil pitch, the vortices become very weak and the flow becomes similar to that of a straight pipe. Additionally, the increase of the curvature ratio ( $\delta$ ; the ratio between pipe diameter  $d$  and the coil diameter  $D$ ,  $\delta = d/D$ ) intensifies the vortices (Mishra and Gupta, 1979; Saxena and Nigam, 1979; Yamamoto et al., 1994; Hüttel and Friedrich, 2000).

According to that, the present study aims to find the optimal Reynolds number for the best separation also for helical pipes with different geometrical parameters. Starting from the first geometry (G1) considered in Mansour et al. (2021), all the key geometrical parameters of the helical pipe were varied and studied, i.e., the pitch of the coil ( $P$ ), the diameter of the pipe ( $d$ ), and the diameter of the coil ( $D$ ). Overall, 7 different helical configurations were studied (G1 to G7), which are similar to those studied in Mansour et al. (2020a) for miscible fluids. The optimal superficial Reynolds number range obtained in Mansour et al. (2021) was kept ( $Re_w=225-563$ ). This corresponds to a superficial Dean number range of water ( $De_w$ ) of approximately  $45 \leq De_w \leq 165$  for all considered helical pipes. The results of the present study deliver optimal geometrical and flow conditions for the separation of immiscible fluids in helical pipes that are widely valid.

## 2 Numerical Modeling

### 2.1 Conservation equations

The continuity and momentum (governing) equations in Cartesian coordinates are given below, considering an unsteady and adiabatic flow as well as Newtonian and incompressible fluids.

Continuity equation:

$$\frac{\partial u_i}{\partial x_i} = 0, \quad (1)$$

Momentum equation:

$$\rho \left( \frac{\partial u_i}{\partial t} + u_j \frac{\partial u_i}{\partial x_j} \right) = -\frac{\partial p}{\partial x_i} + \frac{\partial}{\partial x_j} \left[ \mu \left( \frac{\partial u_i}{\partial x_j} + \frac{\partial u_j}{\partial x_i} \right) \right] + \rho g_i + f_b, \quad (2)$$

where  $i = 1, 2, 3$  and represents the three coordinates,  $p$  is the pressure,  $u$  is the flow velocity,  $\mu$  is the dynamic viscosity of the fluid,  $\rho$  is the density of the fluid,  $g$  is the acceleration due to gravity, and  $f_b$  is the body force.

### 2.2 Modeling of immiscible phases

The Volume Of Fluid (VOF) model was used to model the interactions and the interface between the two immiscible liquids, considering here the flow of amine and water. The VOF model solves a scalar transport equation for the local volume fraction ( $\alpha$ ) of the phases. Eq. 3 presents the scalar transport equation of the volume fraction ( $\alpha_m$ ) of a phase  $m$ .

$$\frac{\partial \alpha_m}{\partial t} + \vec{u} \cdot \frac{\partial \alpha_m}{\partial x_i} = 0 \quad (3)$$

All the different phases are modeled in the VOF model by solving one set of conservation equations (also known as one-fluid formulation), considering common velocity, pressure, and temperature fields. This VOF technique leads to very good results regarding immiscible fluid flow as approved by several studies (Mansour et al., 2021, 2020d; Koppaarthi et al., 2020; Parikh et al., 2020; Mansour et al., 2020e).

The volume fraction of the phase  $m$  in a flow of  $k$  phases ( $k = 2$  for a flow of two phases as the one considered here) can be calculated by:

$$\alpha_m = \frac{V_m}{V} \quad (4)$$

where,  $V_m$  is the occupied volume by the phase  $m$  in the computational cell, and  $V$  is the total volume of the computational cell. This implies that the summation of the volume fractions of all phases is equal to one. A value of  $\alpha_m = 0$  or  $\alpha_m = 1$  means that the phase  $m$  is not existing in the computational cell or the phase  $m$  occupies the computational cell completely. If the phase volume fraction is between 0 and 1 ( $0 < \alpha_m < 1$ ), the computational cell is partially occupied by the phase  $m$ , where a local interface between the phases is also present in the computational cell. The mixture properties are calculated based on the volume fraction of phases for the computation cells having an interface. In this way, the fluid phases can be characterized in a computational cell according to their volume fractions.

### 2.3 Quantification of phase separation

The separation performance was quantified by the mixing coefficient ( $M_c$ ) (Mansour et al., 2017, 2020a,d, 2021), which denotes how uniform the liquid phases are distributed over a specific cross-sectional area. For the phase  $m$ , the mixing coefficient over a cross-sectional area of  $A$  can be obtained by:

$$M_{c\ m} = 1 - \frac{\sum_f |\alpha_m - \bar{\alpha}_m| A_f}{|\bar{\alpha}_m| \sum_f A_f} \quad (5)$$

and

$$\bar{\alpha}_m = \frac{1}{A} \int \alpha_m dA \quad (6)$$

where  $\bar{\alpha}_m$  is the surface-averaged volume fraction of phase  $m$  over the cross-sectional area  $A$ , and  $A_f$  is the area of a computational cell face. The mixing coefficient was evaluated for each liquid individually, and then the two values were averaged, representing the overall mixing coefficient  $M_c$ . As mentioned before, the two liquids were assumed to be totally dispersed in one another (perfectly mixed, 100% mixing) at the inlet of the helical pipes ( $M_c = 1$ ) with a volume fraction of 0.5 for each liquid. This condition corresponds to the theoretical worst situation for the two liquids to separate since the liquids will separate faster in case of partial dispersion between the liquids (Zhang et al., 2006).

### 2.4 Numerical settings

The computational fluid dynamics code Star-CCM+ was employed in the present work to study the flow in the helical pipes. An unsteady, implicit, and segregated solver as well as a laminar setup were used. A second-order upwind convection scheme was used for space discretization, while a first-order upwind scheme was set for temporal discretization. An adaptive time step (variable time step between approximately  $2 \times 10^{-4}$  and  $8 \times 10^{-4}$  s) was set to ensure that the maximum local CFL (Courant–Friedrichs–Lewy) number is always not exceeding 1. For calculating the maximum local CFL number, the smallest cell size of the whole domain and the highest velocity were used. For guaranteeing enough drop of all absolute residuals, 10 iterations were set per time step. A total physical time of 1.5 of the average residence time of the fluids in the pipes was considered, ensuring that the flow reached quasi-steady conditions before ending the simulation and analyzing the results. The physical time considered varies for all the considered cases between 20 and 75 seconds. For the pipe walls, a no-slip velocity boundary condition and zero-gradient conditions for the scalar fields were set. A realistic Hagen-Poiseuille (parabolic) velocity distribution was imposed at the inlet of all helical pipes. In this way, the numerical errors related to the assumption of plug-flow (uniform velocity distribution) at the inlet could be eliminated (Mansour et al., 2017). Finally, a constant-pressure boundary condition was set at the outlet of the helical pipes.

### 2.5 Helical geometries

Fig. 1 illustrates the helical pipe (first geometry; G1) in vertical upward, vertical downward, and horizontal flow orientations, representing the orientations studied. The helical parameters of the first helical pipe geometry (G1) were selected according to an available experimental prototype, which was employed and studied in various previous papers (Jokiel et al., 2017; Mansour et al., 2017, 2020a, 2019b; Khot et al., 2019; Kováts et al., 2020b; Mansour et al., 2021, 2020c). Starting from this first geometry (G1), all the helical pipe dimensions geometrical were changed in a wide enough range to significantly affect the secondary flow (Mansour et al., 2020g). Three different values were studied for each geometrical parameter, i.e., the pitch of the coil ( $P$ ), the diameter of the pipe ( $d$ ), and the diameter of the coil ( $D$ ). Note that, the impact of the pipe diameter ( $d$ ) and the coil diameters ( $D$ ) were considered individually, since they influence the flow features differently (Tang et al., 2017; Mohammed and Narrein, 2012; Cioncolini and Santini, 2006; Mansour et al., 2020a,g). Among G1, G2 and G3, the coil pitch ( $P$ ) values are 16, 30, and 60 mm, respectively. Similarly, the pipe diameter ( $d$ ) values of G4, G1, and G5 are 5, 10, and 15 mm, respectively. Finally, the coil diameter ( $D$ ) values of G6, G1, and G7 are 70, 118, and 150 mm, respectively. This led to 7 different helical pipes similar to those studied in Mansour et al. (2020a) for miscible fluids. Fig. 2 and Tab. 1 present the dimensions and the details of the 7 different helical pipes. Here, the curvature ratio ( $\delta = d/D$ ) and the dimensionless pitch ( $\gamma = P/\pi D$ ) values are also given in Tab. 1. For G1, a number of coil turns of  $n = 3$  were found enough to investigate the separation (Mansour et al., 2021). Nonetheless, to provide a fair comparison among different helical pipes, the total pipe length ( $L = n\sqrt{(\pi D)^2 + P^2} = 1113$  mm) was kept approximately similar by adjusting the number of coil turns. This was mainly done for G6 and G7 (see again Tab. 1 and Fig. 2).

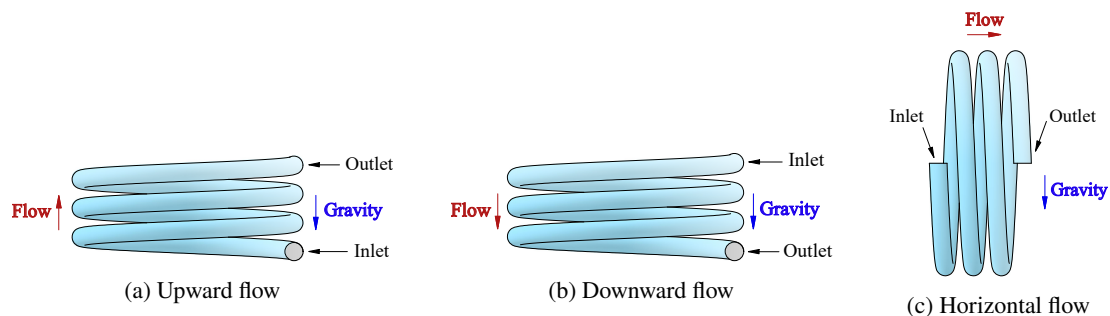
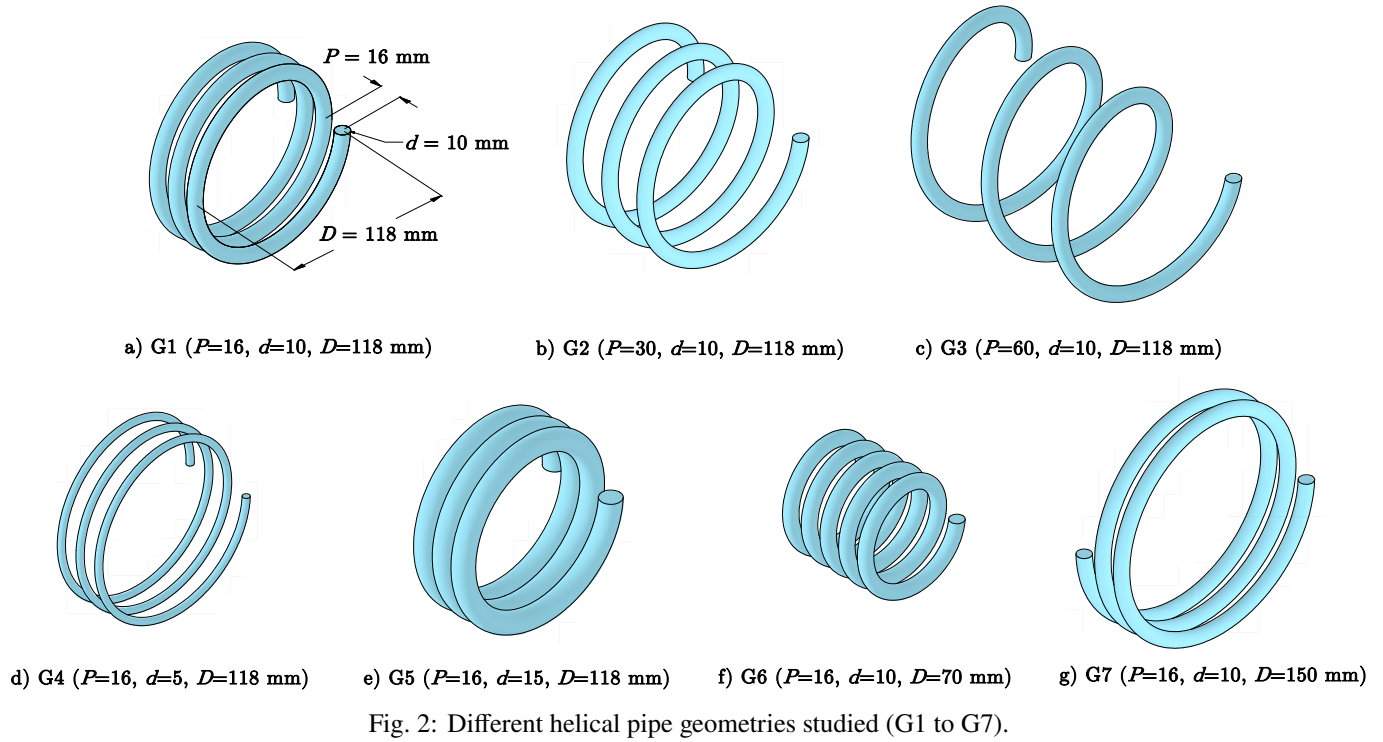


Fig. 1: Illustration of different flow orientations studied.



## 2.6 Flow and physical conditions

The two immiscible liquids investigated are amine and water. This two-phase flow is related to the hydroformylation process (Mansour et al., 2021; Jokiel et al., 2019). The physical properties of the liquids are listed in Tab. 2. The surface tension force between the liquids was considered in the simulations, where the surface tension coefficient was set to 0.0285 N/m (Mansour et al., 2021).

As stated before, the optimal values of Reynolds number for separation (Mansour et al., 2021) were kept, i.e.,  $Re_w = 225$ -563, where  $Re_w$  is the superficial Reynolds number of water given in Eq. 7. Similarly,  $Re_a$  is the superficial Reynolds number of amine given in Eq. 8.

$$Re_w = \frac{\rho_w v d}{\mu_w} \quad (7)$$

$$Re_a = \frac{\rho_a v d}{\mu_a} \quad (8)$$

Tab. 3, lists the simulation cases (flow conditions) investigated. As can be seen in Tab. 3, initially two cases (Case 1 and Case 2) were considered for G1 ( $Re_w = 225$  and  $Re_w = 563$ ). Nevertheless, a value of  $Re_w = 225$ , was kept for all the other geometries since it resulted in slightly better phase separation. In Tab. 3,  $v$  represents the average velocity of the flow, which was set at the pipe inlet to change the Reynolds number value. The corresponding values of the Dean number are also given in Tab. 3 for each phase, where

$$De_a = Re_a \sqrt{\delta} \quad (9)$$

$$De_w = Re_w \sqrt{\delta} \quad (10)$$

In the following, only the superficial Reynolds number of water ( $Re_w$ ) will be given to represent the case, since it is always bigger than that of the amine phase.

Tab. 1: Geometrical parameters of the different helical pipes studied (G1 to G7).

Coil	$P$ mm	$d$ mm	$D$ mm	$L$ mm	$\delta = d/D$	$\gamma = P/\pi D$	$n$
G1	16	10	118	1113	0.084	0.043	3
G2	30	10	118	1115	0.084	0.081	3
G3	60	10	118	1126	0.084	0.162	3
G4	16	5	118	1113	0.042	0.043	3
G5	16	15	118	1113	0.127	0.043	3
G6	16	10	70	1102	0.142	0.0727	5
G7	16	10	150	1178	0.066	0.034	2.5

Tab. 2: Physical properties of the immiscible liquids.

	Amine	Water
Density (kg/m <sup>3</sup> )	$\rho_a = 791$	$\rho_w = 999.79$
Dynamic viscosity (Pa·s)	$\mu_a = 1.99 \cdot 10^{-3}$	$\mu_w = 8.887 \cdot 10^{-4}$

Tab. 3: Different flow conditions considered.

Case #	Coil	$v$ (m/s)	$Re_a$	$Re_w$	$De_a$	$De_w$
1	G1	0.05	199	563	58	164
2	G1	0.02	79	225	23	65
3	G2	0.02	79	225	23	65
4	G3	0.02	79	225	23	65
5	G4	0.04	79	225	16	46
6	G5	0.0133	79	225	28	80
7	G6	0.02	79	225	28	80
8	G7	0.02	79	225	20	58

## 2.7 Computational grid

After a grid-independence study, the grid size was selected, confirming grid-independent results (Mansour et al., 2021, 2019a). For the different geometries (G1 to G7) geometrical scale factors were applied to always create grids with the same cell size. This ensures a constant resolution in space for all different helical pipes. Finally, structured hexahedral elements (aligned with the flow direction) were created with a minimum of approximately 0.85 million cells for G4 and a maximum of approximately 3.1 million cells for G5. An example of the used grid for G1 is illustrated in Fig. 3.

## 3 Results and Discussions

### 3.1 Time averaging

Since the considered two-phase flow is unsteady, different flow patterns pass through the pipe for each time instance. Accordingly, the mixing coefficient  $M_c$  calculated on a certain pipe section fluctuates instantaneously with time. Therefore, the mixing coefficient was averaged over a certain period of time. The time period needed for stable averaged values was checked. Changes were seen in the averaged values for time periods smaller than 3 seconds. However, for time periods bigger than 3.5 seconds, stable values are observed. The time-averaged  $M_c$  over 3.5 and 5 seconds is shown in Fig. 4 as a function of the axial length of helical pipe G1. As can be observed, these two time periods result in almost identical behaviors. Thus, the time-averaged mixing coefficient was calculated for all the following simulations over a time period of 3.5 seconds.

### 3.2 Impact of flow orientation

Fig. 5a, 5b, 5c compares the separation behavior for the three considered flow orientations, i.e., vertical upward, vertical downward, and horizontal, respectively. In Fig. 5, the volume fraction of amine is shown at  $Re_w = 563$  in G1. Note that, green denotes the perfect mixture of the two liquids as set at the pipe inlet. Pure water is shown in blue (zero volume fraction of amine). Further, the separated amine phase is shown by red iso-surfaces, highlighting all grid cells with a volume fraction of amine higher than or equal to 0.99. As shown, the liquids do not separate properly for the two vertical cases. For instance, only a narrow layer of water (the denser phase) accumulates very slowly on the lower side of the pipe for the vertical upward flow presented in Fig. 5a. Similarly, for the vertical downward flow case presented in Fig. 5b, only very restricted separation takes place after two helical

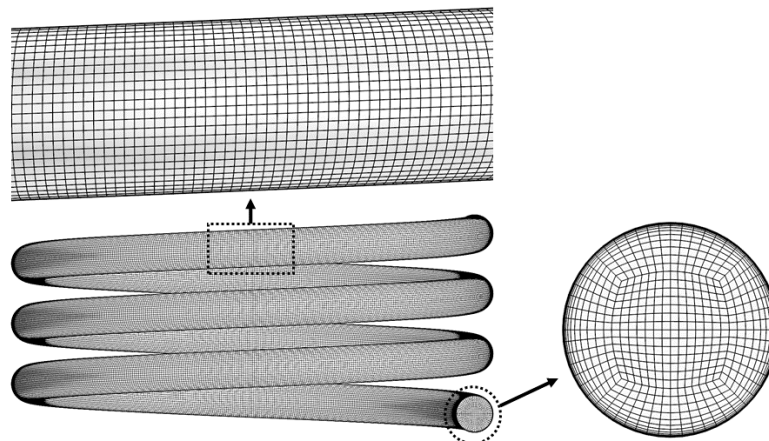


Fig. 3: Example of the used hexahedral grid (Here, G1 is shown with approximately 1.85 million cells).

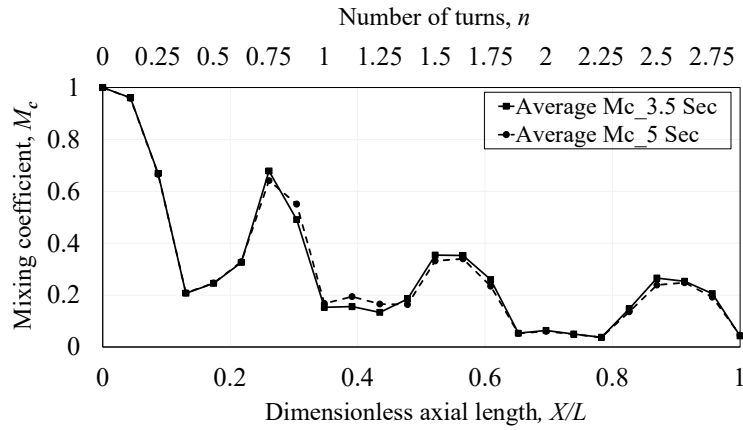


Fig. 4: Time-averaged  $M_c$  over two different time periods (3.5 or 5 seconds) for G1 at  $Re_w = 563$  with horizontal flow orientation.

turns. Conversely, the phase separation occurs when the helical pipe is oriented horizontally as illustrated in Fig. 5c, where amine accumulates quickly after no more than one helical turn. As shown, the amine is also accumulating at the end of every helical turn. The reason for the occurrence of this separation in the horizontal orientation of the helical pipe is that the relative direction between the flow and the buoyant force changes each half helical turn. This forces the lighter liquid to accumulate before the locations of maximum pressure, i.e., the lowest point of each helical turn.

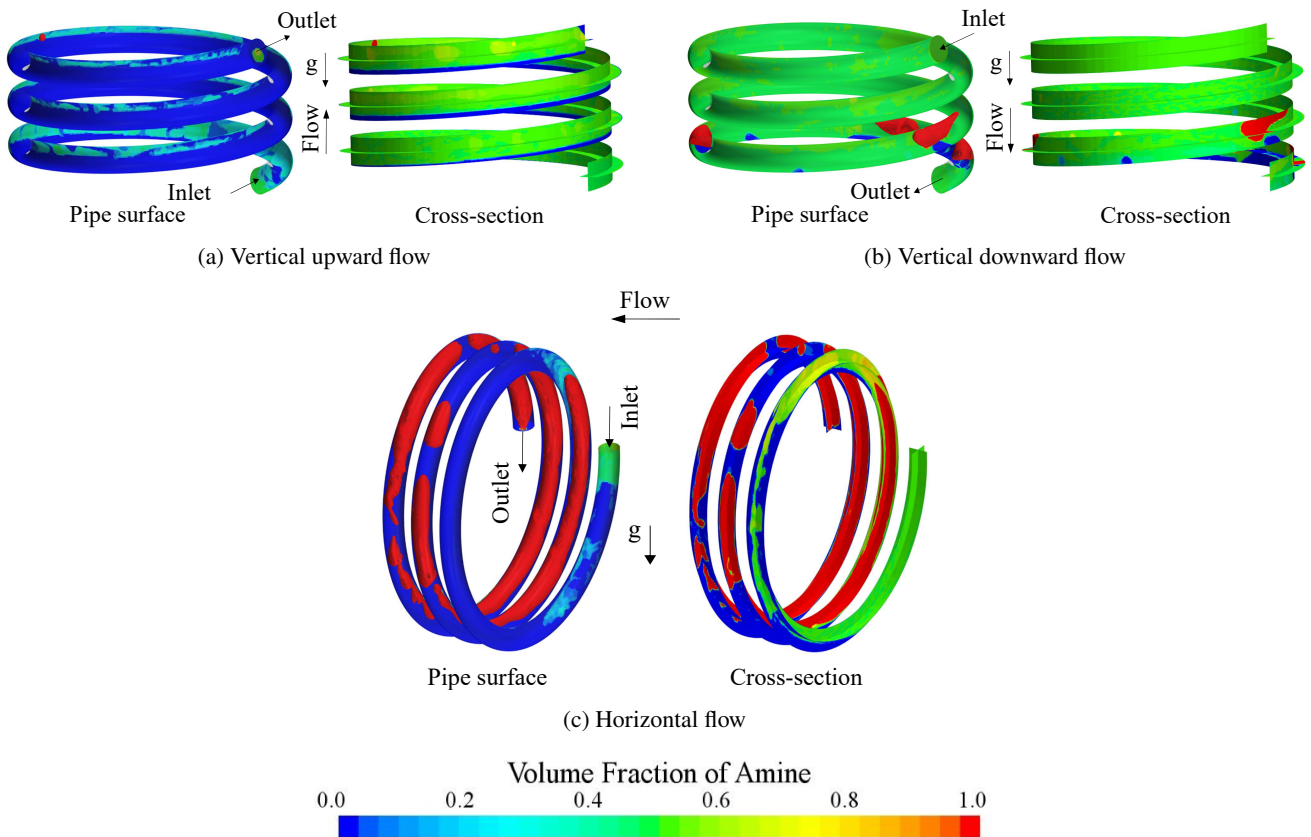


Fig. 5: Amine volume fraction at  $Re_w = 563$  in G1, (a) Vertical upward flow, (b) Vertical downward flow, and (c) Horizontal flow.

Fig. 6 shows the evolution of the mixing coefficients along the helical pipe length for the three flow orientations studied in the first helical pipe (G1) at  $Re_w = 563$ . In each plot, three curves are shown, which are representing the minimum, the time-averaged, and the maximum mixing coefficient. As observed in Fig. 6a, the curves go down as a result of the gradual accumulation of the denser phase on the bottom side of the pipe. However, the two liquids stay mostly mixed till the pipe outlet. This is also the case for the vertical downward orientation demonstrated in Fig. 6b, whereas some oscillations are seen in the curves near the pipe end as a result of the separation of some slugs and big droplets of amine. Overall, the separation is very limited for the vertical flow. Though the mixing coefficient curves oscillate along the helical pipe length for the horizontal case in Fig. 6c, the values drop down to 0.04 near the end of the second helical turn. Also, the variation range between the three curves is very limited, confirming very proper separation of the phases in the horizontal case. Note that, the oscillation of the curves occurs as a result of the presence of local accumulations of the lighter phase at some locations together with mixed two-phase flow at other locations of the pipe. Even so, very good separation takes place in the horizontal helical pipe at the accumulation regions.

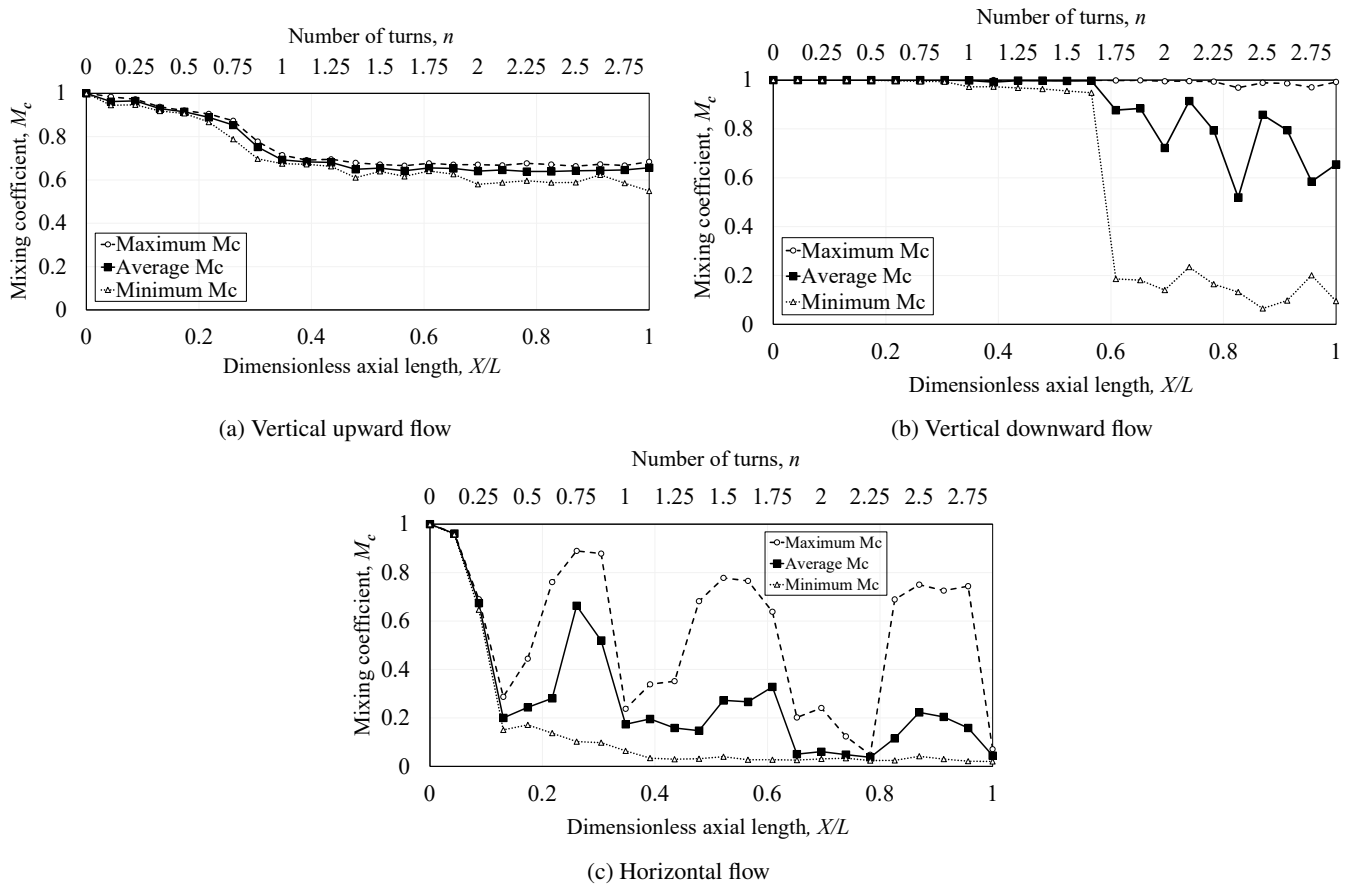


Fig. 6: Evolution of the mixing coefficients along the length of the helical pipe at  $Re_w = 563$  in G1.

### 3.3 Impact of Reynolds number

In Fig. 7, the volume fraction of amine is shown for  $Re_w = 225$  and  $Re_w = 563$  in the first geometry (G1) to explain the impact of Reynolds number. For both cases, the lighter phase accumulates and phase separation occurs properly. However, bigger accumulations and slightly better separation can be seen for the lower value of the Reynolds number because of the higher residence time available for the flow to separate. Several similarities can be seen in the mixing coefficient curves for both values as shown in Fig. 8. Nevertheless, the improved separation for  $Re_w = 225$  is clearly observed at the end of the second coil turn at approximately  $X/L \approx 0.6 - 0.8$ , where the three mixing coefficient curves are very close to zero. Accordingly, a Reynolds number value of  $Re_w = 225$  was kept for further simulations to study the influence of the geometrical parameters.

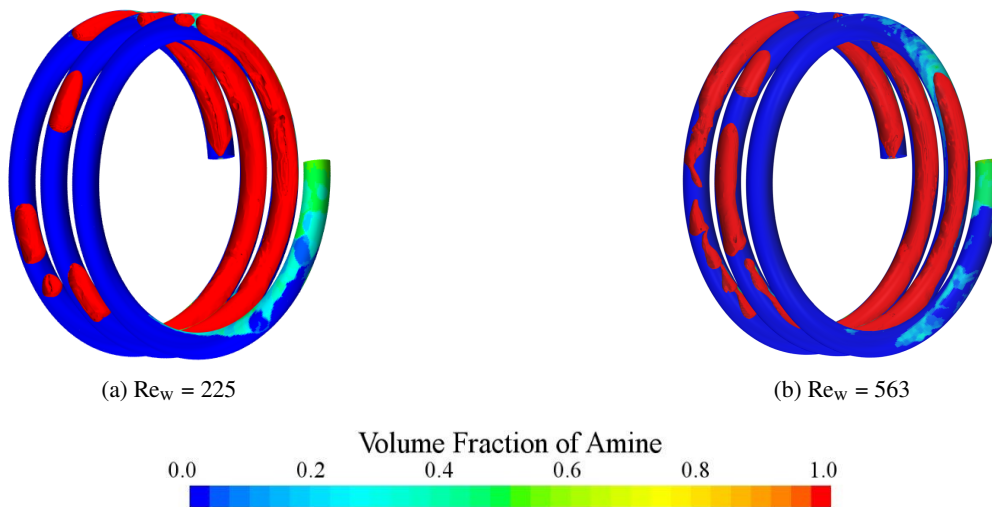


Fig. 7: Amine volume fraction for horizontal flow orientation at (a)  $Re_w = 225$  and (b)  $Re_w = 563$  in G1.

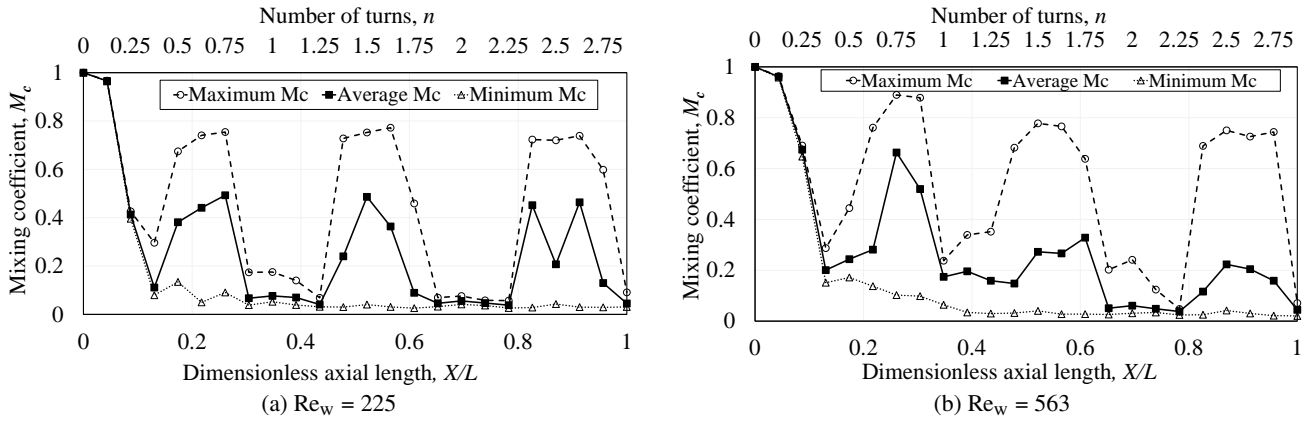


Fig. 8: Evolution of mixing coefficients along the length of the helical pipe at (a)  $Re_w = 225$  and (b)  $Re_w = 563$  in G1.

### 3.4 Impact of geometrical parameters

#### 3.4.1 Impact of coil pitch ( $P$ )

Now, the phase separation is examined at  $Re_w=225$ , when the coil pitch ( $P$ ) is changed among G1, G2, and G3 from 16, to 30, and then to 60 mm, respectively. In Fig. 9, very good phase separation takes place for all three different pitch values. Only minor changes in the flow pattern can be observed. The reason for the similar separation behavior among the different coil pitch values is that the separation takes place while the flow is moving down facing the maximum pressure point at the bottom, which is not affected when increasing the coil pitch in the horizontal direction. The separation behavior is also very similar when comparing the mixing coefficient curves for different values of coil pitch as presented in Fig. 10 (see again Fig. 8a for G1,  $P = 16$  mm).

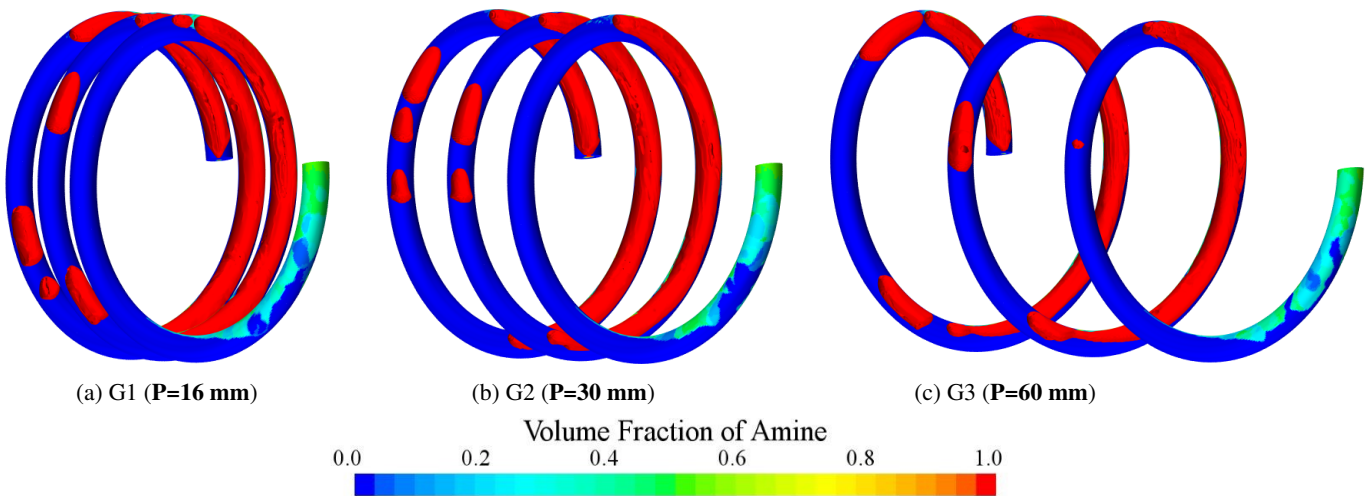


Fig. 9: Amine volume fraction at  $Re_w = 225$  in (a) G1, (b) G2, and (c) G3.

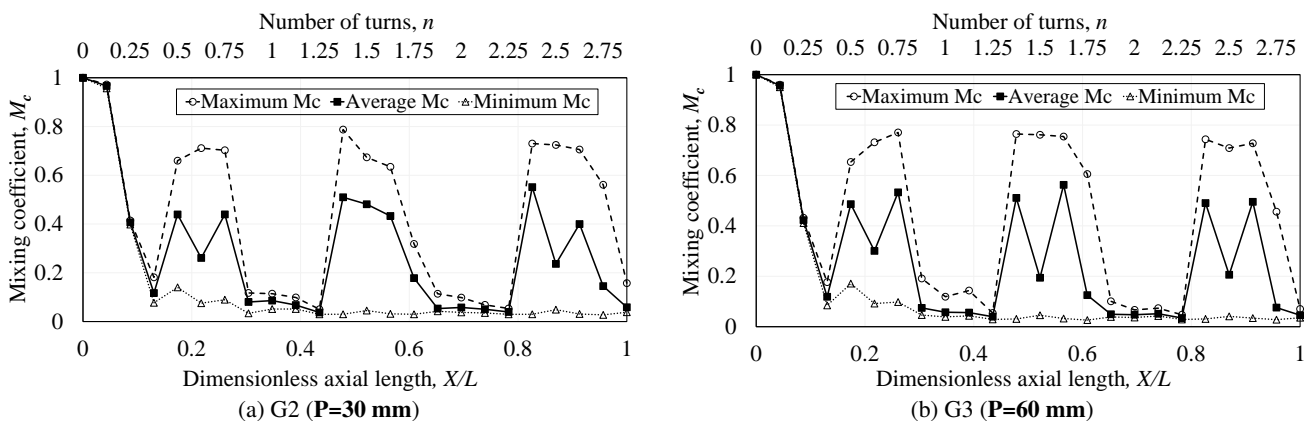


Fig. 10: Evolution of mixing coefficients along the length of helical pipe at  $Re_w = 225$  in (a) G2 and (b) G3.

For more accurate comparisons of the whole separation behavior for different pitch values, the integrated areas under the mixing coefficient curves of Fig. 8a, 10a, and 10b are compared in Fig. 11. The trapezoidal method was used to numerically integrate the area under the mixing coefficient curves. Fig. 11 confirms that the optimal value of  $Re_w=225$  is also valid for widely different coil pitch values, where the good separation performance is not impacted.

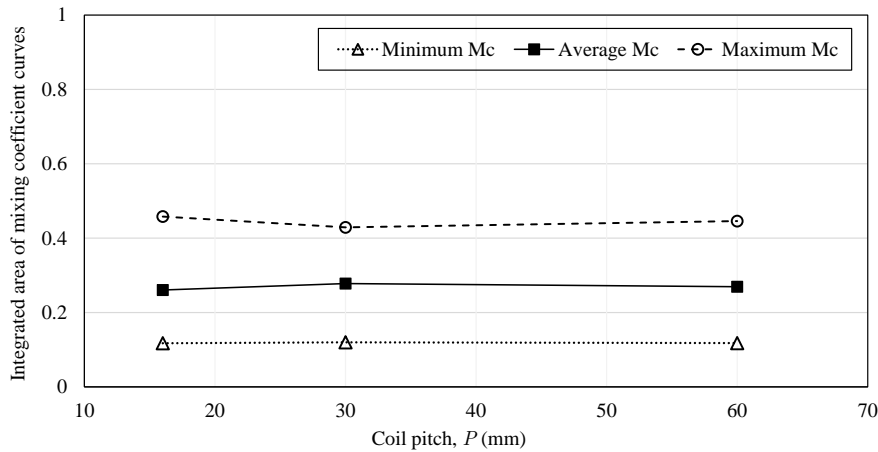


Fig. 11: Integrated areas under the mixing coefficient curves as a function of coil pitch ( $P$ ).

### 3.4.2 Impact of pipe diameter ( $d$ )

Similarly, the phase separation is compared at  $Re_w=225$  between G4, G1, and G5 with pipe diameters ( $d$ ) of 5, 10, and 15 mm, respectively. Fig. 12 shows the amine volume fraction for the three helical geometries. Here, a strong impact on the separation behavior can be seen when the pipe diameter is changed. For the lowest pipe diameter (G4 shown in Fig. 12a), the phase separation does not take place properly, where a change in the flow pattern takes place. The accumulated amine disappears and a plug flow is generated after approximately two helical turns. The higher flow velocity (see again Case 5 in Tab. 3) and the lower residence time are the main reasons for the sharply reduced separation. On the other hand, the separation is moderately improved when the pipe diameter is increased as shown for G5 in Fig. 12c. The lower flow velocity and the higher residence time in G5 are again the reasons for this enhanced separation. The reduced and improved separation behaviors of G4 and G5, respectively, are directly reflected in Fig. 13 on the mixing coefficients along the axial pipe length. The integrated areas under the mixing coefficient curves of Fig. 13a and 13b together with Fig. 8a are compared in Fig. 14. As shown, the areas are very high for the lowest pipe diameter, indicating very poor phase separation in G4. Nevertheless, a very good separation is still preserved for the other two pipe diameters (G1 and G5) at the optimal value of  $Re_w=225$ .

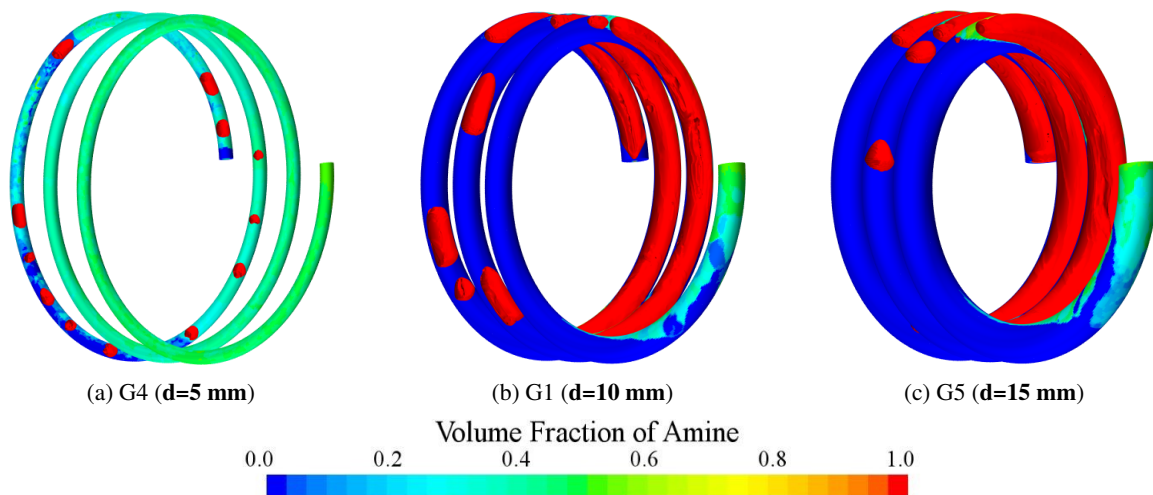


Fig. 12: Amine volume fraction at  $Re_w = 225$  in (a) G4, (b) G1, and (c) G5.

### 3.4.3 Impact of coil diameter ( $D$ )

Finally, the impact of the coil diameter ( $D$ ) on the phase separation is compared at  $Re_w=225$  between G6, G1, and G7 with coil diameters ( $D$ ) of 70, 118, and 150 mm, respectively. Fig. 15 compares the amine volume fraction for the three helical geometries: G6, G1, and G7. Overall, accumulations of amine and proper separation can be seen at the end of each helical turn for the three geometries. However, for the lowest coil diameter (G6 shown in Fig. 15a), a shorter length of accumulations is seen due to the short vertical span available for the flow, where the accumulations are distributed axially over 5 helical turns. On the other hand,

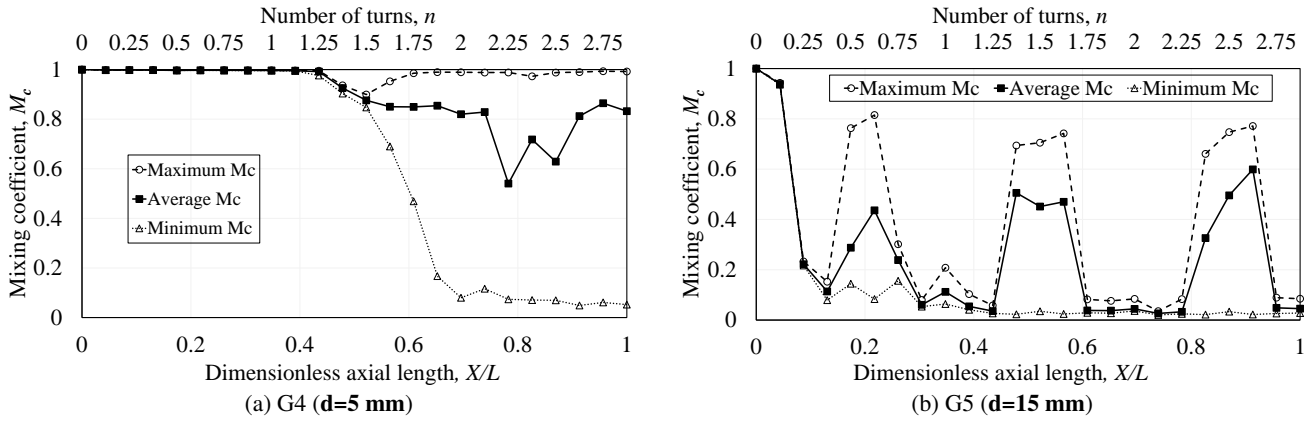


Fig. 13: Evolution of mixing coefficients along the length of helical pipe at  $Re_w = 225$  in (a) G4 and (b) G5.

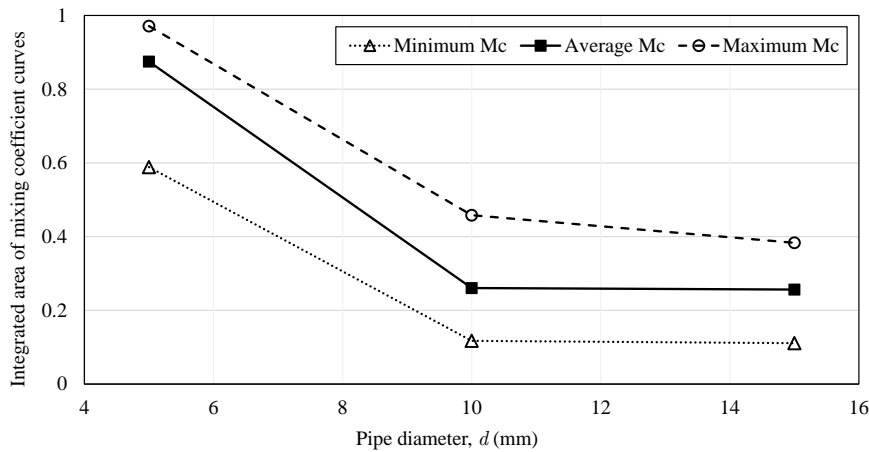


Fig. 14: Integrated areas under the mixing coefficient curves as a function of pipe diameter ( $d$ ).

the accumulations become longer as the coil diameter is increased as shown for G1 and G7 in Fig. 15b and Fig. 15c, respectively. This can be beneficial concerning separation since extracting the lighter phase would be easier in this case with fewer locations of extraction. The separation behaviors of G6 and G7 are presented in Fig. 16, where the mixing coefficient curves of G6 show more peaks and valleys due to the distributed accumulations of amine. Fig. 17 shows the integrated areas under the mixing coefficient curves for G6, G1, and G1. Here, it can be seen that the overall separation is also improved as the coil diameter increases. According to the presented results, it would be generally recommended to employ helical pipes with a horizontal flow orientation at a Reynolds number of approximately 225. Varying the coil pitch is not very influential concerning the phase separation, while the pipe and coil diameters should be kept high enough to ensure efficient separation of immiscible liquids and easier extraction of the lighter phase.

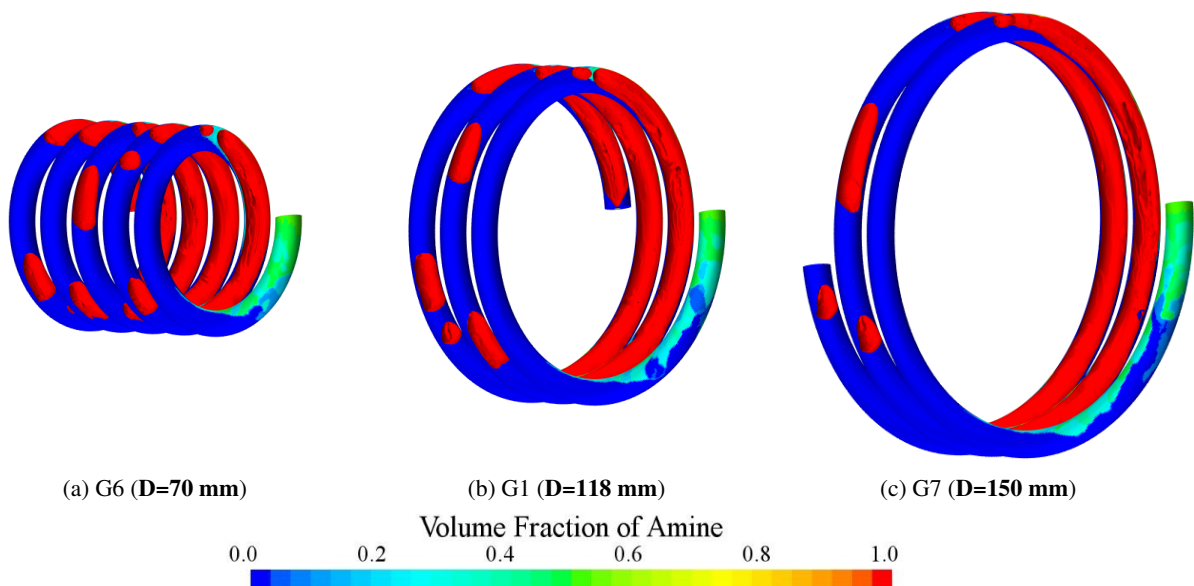


Fig. 15: Amine volume fraction at  $Re_w = 225$  in (a) G6, (b) G1, and (c) G7.

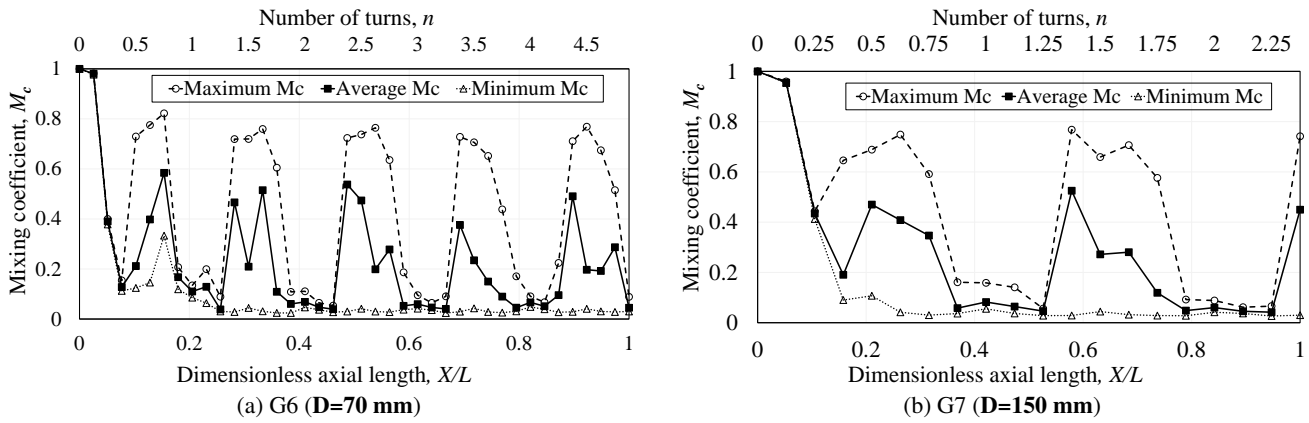


Fig. 16: Evolution of mixing coefficients along the length of helical pipe at  $Re_w = 225$  in (a) G6 and (b) G7.

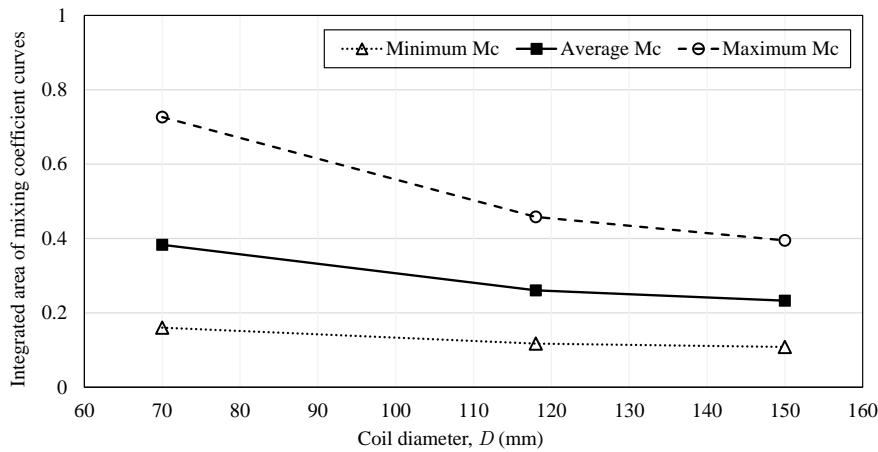


Fig. 17: Integrated areas under the mixing coefficient curves as a function of coil diameter ( $D$ ).

## 4 Conclusions

Immiscible liquids separation was studied in helical pipes considering various flow and geometrical conditions. The Volume Of Fluid (VOF) method was used to model the two-phase flow. The average mixing coefficient was utilized to quantify and compare the separation behavior among the different studied cases. A perfect mixture of two liquids (water and amine) was always assumed at the inlet since it represents the worst theoretical case for the two liquids to separate. Very proper separation could be obtained when the helical pipe is oriented horizontally, while the vertical upward and the vertical downward flows led to very weak phase separation. Two values of Reynolds number (225 and 563) were considered, representing the optimal range. The lower value resulted in a slightly better separation due to the higher residence time available for the flow. The impact of all the geometrical dimensions of helical pipes was also considered. The separation behavior does not change when the coil pitch is varied widely between 16 and 60 mm. However, the pipe and coil diameters have significant impacts on the phase separation, where the separation is generally improved when either the pipe diameter or the coil diameter is increased with the studied ranges of 5–15 mm and 70–150 mm, respectively. Accordingly, horizontal orientation is generally recommended. A Reynolds number of approximately 225 is also preferred. The coil pitch value can be varied freely, while the pipe and coil diameters should be adequately high to ensure efficient separation of immiscible liquids.

## Acknowledgment and Funding Information

The authors would like to thank the Deutsche Forschungsgemeinschaft (DFG, German Research Foundation) - TRR 63 “Integrated Chemical Processes in Liquid Multiphase Systems” (subproject B1) - 56091768 (Gefördert durch die Deutsche Forschungsgemeinschaft (DFG) - TRR 63 “Integrierte chemische Prozesse in flüssigen Mehrphasensystemen” (Teilprojekt B1) – 56091768).

## References

- N. Acharya, M. Sen, and C. Hsueh-Chia. Heat transfer enhancement in coiled tubes by chaotic mixing. *Int. J. Heat Mass Transf.*, 35(10):2475–2489, 1992.
- M. Al-Azzawi, F. S. Mjalli, A. Husain, and M. Al-Dahhan. A review on the hydrodynamics of the liquid–liquid two-phase flow in the microchannels. *Ind. Eng. Chem. Res.*, 60(14):5049–5075, 2021.

- N. Ali and M. M. Mandal. Immiscible liquid-liquid flow in coiled tube. In *International Conference on Sustainable and Innovative Solutions for Current Challenges in Engineering & Technology*, pages 307–319. Springer, 2019.
- N. Brauner and D. M. Maron. Flow pattern transitions in two-phase liquid-liquid flow in horizontal tubes. *Int. J. Multiph. Flow*, 18(1):123–140, 1992.
- A. Cioncolini and L. Santini. An experimental investigation regarding the laminar to turbulent flow transition in helically coiled pipes. *Exp. Therm. Fluid Sci.*, 30(4):367–380, 2006. ISSN 0894-1777.
- C. T. Culbertson, S. C. Jacobson, and J. M. Ramsey. Microchip devices for high-efficiency separations. *Anal. Chem.*, 72(23):5814–5819, 2000.
- F. R. M. da Mota and D. J. Pagano. Simulation and experimental study of phase segregation in helical pipes: A new method for flow conditioning. *Flow Meas. Instrum.*, 35:99–108, 2014.
- W. R. Dean. Note on the motion of fluid in a curved pipe. *Lond. Edinb. Dubl. Phil. Mag.*, 4(20):208–223, 1927. ISSN 1941-5982.
- A. Y. Gelfgat, A. L. Yarin, and P. Z. Bar-Yoseph. Dean vortices-induced enhancement of mass transfer through an interface separating two immiscible liquids. *Phys. Fluids*, 15(2):330–347, 2003.
- R. L. Hartman, H. R. Sahoo, B. C. Yen, and K. F. Jensen. Distillation in microchemical systems using capillary forces and segmented flow. *Lab Chip*, 9(13):1843–1849, 2009.
- T. J. Hüttl and R. Friedrich. Influence of curvature and torsion on turbulent flow in helically coiled pipes. *Int. J. Heat Fluid Flow*, 21(3):345–353, 2000. ISSN 0142-727X.
- T. J. Hüttl and R. Friedrich. Direct numerical simulation of turbulent flows in curved and helically coiled pipes. *Comput. Fluids*, 30(5):591–605, 2001. ISSN 0045-7930.
- F. Jiang, K. S. Drese, S. Hardt, M. Küpper, and F. Schönfeld. Helical flows and chaotic mixing in curved micro channels. *AIChE J.*, 50(9):2297–2305, 2004.
- M. Jokieli, L. M. Wagner, M. Mansour, N. M. Kaiser, K. Zähringer, G. Janiga, K. D. P. Nigam, D. Thevenin, and K. Sundmacher. Measurement and simulation of mass transfer and backmixing behavior in a gas-liquid helically coiled tubular reactor. *Chem. Eng. Sci.*, 170:410–421, 2017.
- M. Jokieli, N. M. Kaiser, P. Kováts, M. Mansour, K. Zähringer, K. D. P. Nigam, and K. Sundmacher. Helically coiled segmented flow tubular reactor for the hydroformylation of long-chain olefins in a thermomorphic multiphase system. *Chem. Eng. J.*, 377:120060, 2019.
- D. S. Juang, S. M. Berry, C. Li, J. M. Lang, and D. J. Beebe. Centrifugation-assisted immiscible fluid filtration for dual-bioanalyte extraction. *Anal. Chem.*, 91(18):11848–11855, 2019.
- P. Khot, M. Mansour, D. Thévenin, K. D. P. Nigam, and K. Zähringer. Improving the mixing characteristics of coiled configurations by early flow inversion. *Chem. Eng. Res. Des.*, 146:324–335, 2019.
- S. Koppaarthi, M. Mansour, G. Janiga, and D. Thévenin. Numerical investigations of turbulent single-phase and two-phase flows in a diffuser. *Int. J. Multiph. Flow*, 130:103333, 2020.
- P. Kováts, D. Pohl, D. Thévenin, and K. Zähringer. Optical determination of oxygen mass transfer in a helically-coiled pipe compared to a straight horizontal tube. *Chem. Eng. Sci.*, 190:273–285, 2018.
- P. Kováts, F. J. W. A. Martins, M. Mansour, D. Thévenin, and K. Zähringer. Tomographic PIV measurements and RANS simulations of secondary flows inside a horizontally positioned helically coiled tube. *Exp. Fluids*, 61(5):1–15, 2020a.
- P. Kováts, C. Velten, M. Mansour, D. Thévenin, and K. Zähringer. Mixing characterization in different helically coiled configurations by laser-induced fluorescence. *Exp. Fluids*, 61(9):1–17, 2020b.
- V. Kumar, M. Aggarwal, and K. D. P. Nigam. Mixing in curved tubes. *Chem. Eng. Sci.*, 61(17):5742–5753, 2006.
- T. M. Liou. Flow visualization and LDV measurement of fully developed laminar flow in helically coiled tubes. *Exp. Fluids*, 13(5):332–338, 1992. ISSN 0723-4864.
- L. Liu, L. Li, Z. Ding, R. Ma, and Z. Yang. Mass transfer enhancement in coiled hollow fiber membrane modules. *J. Membr. Sci.*, 264(1-2):113–121, 2005.
- M. Mansour, Z. Liu, G. Janiga, K. D. P. Nigam, K. Sundmacher, D. Thévenin, and K. Zähringer. Numerical study of liquid-liquid mixing in helical pipes. *Chem. Eng. Sci.*, 172:250–261, 2017.
- M. Mansour, G. Janiga, K. D. P. Nigam, D. Thévenin, and K. Zähringer. Numerical study of heat transfer and thermal homogenization in a helical reactor. *Chem. Eng. Sci.*, 177:369–379, 2018. ISSN 00092509.
- M. Mansour, P. Khot, P. Kováts, D. Thévenin, K. Zähringer, and G. Janiga. Impact of computational domain discretization and gradient limiters on CFD results concerning liquid mixing in a helical pipe. *Chem. Eng. J.*, In Press, (2019):123121, 2019a.
- M. Mansour, D. Thévenin, K. D. P. Nigam, and K. Zähringer. Generally-valid optimal Reynolds and Dean numbers for efficient liquid-liquid mixing in helical pipes. *Chem. Eng. Sci.*, 201:382–385, 2019b. ISSN 0009-2509.
- M. Mansour, P. Khot, D. Thévenin, K. D. P. Nigam, and K. Zähringer. Optimal Reynolds number for liquid-liquid mixing in helical pipes. *Chem. Eng. Sci.*, 214:114522, 2020a.
- M. Mansour, A. Landage, P. Khot, K. D. P. Nigam, G. Janiga, D. Thévenin, and K. Zähringer. Numerical study of gas-liquid two-phase flow regimes for upward flow in a helical pipe. *Ind. Eng. Chem. Res.*, 59(9):3873–3886, 2020b.

- M. Mansour, C. Müller, D. Thévenin, and K. Zähringer. Investigations on the separation of two immiscible liquids in helical pipes with different conditions and dimensions. In *Proc. Conference on Modelling Fluid Flow (CMFF'22), Budapest, Hungary*, pages 430–437, 2020c.
- M. Mansour, T. Parikh, S. Engel, B. Wunderlich, and D. Thévenin. Numerical investigations of gas-liquid two-phase flow in a pump inducer. *J. Fluids Eng.*, 142(2):021302–1–021302–12, 2020d.
- M. Mansour, T. Parikh, and D. Thévenin. Influence of blade pitch and number of blades of a pump inducer on single and two-phase flow performance. In *ASME Turbo Expo 2020: Turbomachinery Technical Conference and Exposition*, page V009T21A010. American Society of Mechanical Engineers, 2020e.
- M. Mansour, D. Thévenin, and K. Zähringer. Numerical study of flow mixing and heat transfer in helical pipes, coiled flow inverters and a novel coiled configuration. *Chemical Engineering Science*, 221:115690, 2020f.
- M. Mansour, K. Zähringer, K. D. P. Nigam, D. Thévenin, and G. Janiga. Multi-objective optimization of liquid-liquid mixing in helical pipes using Genetic Algorithms coupled with Computational Fluid Dynamics. *Chem. Eng. J.*, 391:123570, 2020g. ISSN 1385-8947.
- M. Mansour, S. Kasetti, D. Thévenin, K. D. P. Nigam, and K. Zähringer. Numerical study of the separation of two immiscible liquids in helical and straight pipes. *Chem. Eng. Process.*, page 108654, 2021.
- P. Mishra and S. N. Gupta. Momentum transfer in curved pipes. 1. Newtonian fluids. *Ind. Eng. Chem. Des. Dev.*, 18(1):130–137, 1979. ISSN 0196-4305.
- H. A. Mohammed and K. Narrein. Thermal and hydraulic characteristics of nanofluid flow in a helically coiled tube heat exchanger. *Int. Commun. Heat Mass Transf.*, 39(9):1375–1383, 2012. ISSN 0735-1933.
- T. Parikh, M. Mansour, and D. Thévenin. Investigations on the effect of tip clearance gap and inducer on the transport of air-water two-phase flow by centrifugal pumps. *Chem. Eng. Sci.*, 218:115554, 2020.
- M. Pietrzak. Flow patterns and volume fractions of phases during liquid-liquid two-phase flow in pipe bends. *Exp. Therm Fluid Sci.*, 54:247–258, 2014.
- A. K. Saxena and K. D. P. Nigam. On rtd for laminar flow in helical coils. *Chem. Eng. Sci.*, 34(3):425–426, 1979.
- M. Sharma, P. Ravi, S. Ghosh, G. Das, and P. K. Das. Studies on low viscous oil–water flow through return bends. *Exp. Therm Fluid Sci.*, 35(3):455–469, 2011.
- J. Steinhoff, E. Charlafti, D. Leleu, L. Reinecke, H. Franken, K. Becker, M. Kalem, M. Sixt, M. Braß, D. Borchardt, W. Bäcker, M. Wegener, S. Maaß, M. Weber, T. Acher, C. Matten, A. Pfennig, M. Kraume, and H. J. Bart. Energy and resource savings through innovative and CFD-based design of liquid/liquid gravity separators. *Chem. Ing. Tech.*, 2021.
- L. Tang, Y. Tang, and S. Parameswaran. A numerical study of flow characteristics in a helical pipe. *Adv. Mech. Eng.*, 8(7):1687814016660242, 2016. ISSN 1687-8140.
- L. Tang, S. Yuan, M. Malin, and S. Parameswaran. Secondary vortex-based analysis of flow characteristics and pressure drop in helically coiled pipe. *Adv. Mech. Eng.*, 9(4):1687814017700059, 2017. ISSN 1687-8140.
- S. P. Vanka, G. Luo, and C. M. Winkler. Numerical study of scalar mixing in curved channels at low reynolds numbers. *AIChE J.*, 50(10):2359–2368, 2004.
- S. Vashisth, V. Kumar, and K. D. P. Nigam. A review on the potential applications of curved geometries in process industry. *Ind. Eng. Chem. Res.*, 47(10):3291–3337, 2008. ISSN 0888-5885.
- J. von Deylen, J. Köpplin, and D. Thévenin. Development and Validation of a Design Tool for an Improved Pitot-Tube Jet-Pump Allowing Continuous Fluid-Fluid Separation. *J. Fluids Eng.*, 144(7), 2022. ISSN 0098-2202. 071401.
- E. Weiwei, K. Pope, and X. Duan. Separation dynamics of immiscible liquids. *SN Appl. Sci.*, 2(12):1–14, 2020.
- B. Xu, X. Zhang, L. Zhao, M. Jiang, L. Liu, and H. Xia. Structure design and preliminary experimental investigation on oil-water separation performance of a novel helix separator. *Sep. Sci. Technol.*, pages 1–12, 2020.
- K. Yamamoto, S. Yanase, and T. Yoshida. Torsion effect on the flow in a helical pipe. *Fluid Dyn. Res.*, 14(5):259–273, 1994. ISSN 0169-5983.
- J. Zhang, J. Guo, D. Gong, L. Wang, C. Tang, and Z. Zheng. An investigation on oil/water separation mechanism inside helical pipes. *J. Hydrodyn.*, 18(1):336–340, 2006.
- Y. Zhang, C. Guo, H. Hou, and G. Xue. Experimental research and numerical simulation on gas-liquid separation performance at high gas void fraction of helically coiled tube separator. *Int. J. Chem. Eng.*, 2014, 2014.